Coupled Ocean–Atmosphere Offshore Decay Scale of Cold SST Signals along Upwelling Eastern Boundaries

MICHAEL A. SPALL

Woods Hole Oceanographic Institution, Woods Hole, Massachusetts

NIKLAS SCHNEIDER

International Pacific Research Center, University of Hawaii, Honolulu, Hawaii

(Manuscript received 2 February 2016, in final form 2 August 2016)

ABSTRACT

A simple analytic model is developed to represent the offshore decay of cold sea surface temperature (SST) signals that originate from wind-driven upwelling at a coastal boundary. The model couples an oceanic mixed layer to an atmospheric boundary layer through wind stress and air–sea heat exchange. The primary mechanism that controls SST is a balance between Ekman advection and air–sea exchange. The offshore penetration of the cold SST signal decays exponentially with a length scale that is the product of the ocean Ekman velocity and a time scale derived from the air–sea heat flux and the radiative balance in the atmospheric boundary layer. This cold SST signal imprints on the atmosphere in terms of both the boundary layer temperature and surface wind. Nonlinearities due to the feedback between SST and atmospheric wind, baroclinic instability, and thermal wind in the atmospheric boundary layer all slightly modify this linear theory. The decay scales diagnosed from two-dimensional and three-dimensional eddy-resolving numerical ocean models are in close agreement with the theory, demonstrating that the basic physics represented by the theory remain dominant even in these more complete systems. Analysis of climatological SST off the west coast of the United States also shows a decay of the cold SST anomaly with scale roughly in agreement with the theory.

1. Introduction

A strong atmospheric pressure gradient in the eastern region of subtropical oceans is commonly found in summer between high pressure over the cool ocean and low pressure over the warm continent. This drives equatorward winds over the eastern ocean, giving rise to offshore Ekman transport in the ocean. This transport at the coast is balanced by the upwelling of cold, nutrient-rich waters from depth. These nutrients seed phytoplankton growth, which forms the foundation for the productive fisheries commonly found in such upwelling regions. The cold water also has a significant impact on the atmospheric boundary layer. Summer conditions tend to be cool over the adjacent land with low-level stratus clouds and fog over the ocean. Even though these clouds reduce the incoming solar radiation, these are also regions of strong heat uptake by the ocean (Edwards and Kelly 2007; Holte et al. 2014). These cold eastern boundary regions are also difficult for coupled climate models to represent (Richter 2015), with the resulting errors in SST, cloud cover, and winds having significant influence on precipitation far from the region of SST bias (Large and Danabasoglu 2006).

Although the upwelling is confined to a relatively narrow band along the coast that is $O(10\,\text{km})$ wide, this cold signal in SST can be seen extending hundreds of kilometers into the basin interior. For example, the annual mean SST from the NOAA high-resolution blended analysis (Fig. 1) shows that cold water is found along the eastern boundary at midlatitudes in most of the major ocean basins.[1] These cold signals decay offshore of the eastern boundary where, far into the interior, the SST is only a weak function of longitude (but remains a function of latitude).

Corresponding author address: Michael Spall, MS#21, 360 Woods Hole Road, Woods Hole, MA 02543.
E-mail: mspall@whoi.edu

[1] This gridded product is provided on a $0.25° \times 0.25°$ grid and is based on data between 1982 and 2010.

DOI: 10.1175/JCLI-D-16-0109.1

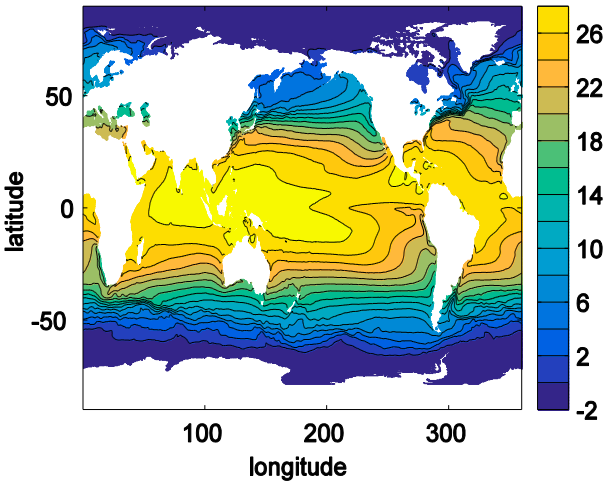

FIG. 1. Annual mean sea surface temperature (°C) from the NOAA high-resolution blended analysis SST dataset.

The along-shore wind stress decays toward the coast so that upwelling is partitioned between the divergences due to the coastal blocking and the offshore increase of the Ekman transport (Dorman et al. 2006). For the California Current, the offshore scale of this wind drop-off varies between 10 and 80 km, and its amplitude between 10% and 80%, and results from a combination of coupled feedbacks, irregularities and capes of the coastline, and coastal topography (Renault et al. 2016a). Renault et al. (2016a) show that the coastal topography and capes are the dominant features. The coupled response to the upwelling cool waters (Chelton et al. 2007) is a minor, but nontrivial, contributor. While the wind drop-off impacts the distribution of cool sea surface temperatures (Capet et al. 2004), the scales of the significant wind drop-off are smaller than the observed offshore scale of the cool upwelled waters of several hundred kilometers. This suggests that leading processes governing the offshore scale of sea surface temperature are found in the oceanic heat budget.

There have been numerous observational and modeling studies that have looked at the heat balance in eastern boundary regions, although a simple and consistent picture has yet to emerge. Marchesiello et al. (2003) used an eddy-resolving regional model to study the dynamics of the California Current System. Very close to the boundary they found a balance between eddy fluxes and mean advection with some heating from the atmosphere, but averaged over 500 km from the coast the primary balance was between mean advection and atmospheric heating, similar to the finding of McCreary et al. (1991). Colas et al. (2012) find that a complex balance of Ekman transport, mean gyre advection, and eddy fluxes is required to balance warming by the atmosphere in the Peru–Chile Current System. Each of these modeling studies produced statistically equilibrated solutions with an offshore decay of the cold SST signal over several hundred kilometers, but the dynamics that determined that offshore decay scale were not explicitly discussed. Edwards and Kelly (2007) explored the seasonal heat budget in the California Current System using satellite and hydrographic data and also found that the dominant balance depended on distance offshore. Within 500 km of the coast, they found that atmospheric heating was balanced by seasonal storage, offshore Ekman transport, and alongshore geostrophic transport, with minor contributions from eddy fluxes except near the coast, where they are more important. In the southeast Pacific, Holte et al. (2014) find that mean gyre advection, Ekman transport, and eddy fluxes are all important in balancing the surface warming. However, this field program was located at 20°S, 85°W, approximately 1000 km offshore and at lower latitude than the strong upwelling off the west coast of the United States.

Most previous theoretical work on wind-driven upwelling has focused on the narrow region where the deep waters are advected to the surface (e.g., Allen 1980; Samelson and de Szoeke 1988; Pedlosky 1978). Details of these models vary in terms of their representation of stratification, mixing, and resolved physics; however, they all produce upwelling from subsurface layers to balance the offshore Ekman transport near the surface. The vertical transport is confined to narrow boundary layers that scale with the baroclinic deformation radius, which is $O(10\,\text{km})$ for these near coastal regions, or the width of the inner shelf. The resulting sloping isopycnals give rise to strong along-boundary currents and the development of bottom boundary layers with onshore transport. However, there has been very little theoretical work done on the large-scale fate of these upwelled cold waters as they are advected offshore.

Observations clearly show that the cold water that upwells along subtropical eastern boundary currents penetrates offshore far beyond the narrow region of upwelling. Modeling studies produce similar hydrography and circulations but have so far not been used to determine what controls this offshore scale. In both model and observational analysis the dominant heat balance finds that surface heating and mean advection are important offshore of the shelf while eddy fluxes have been found at times to be important, especially near the coast, but not consistently so. The primary objective of this study is to provide a basic understanding of what controls this offshore decay scale. While processes not included in the theory may be important in some regions, the simple model developed

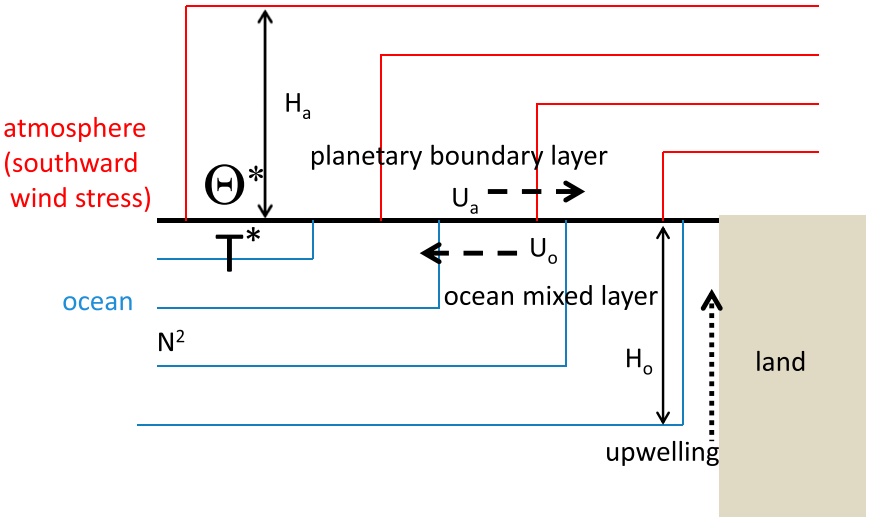

FIG. 2. Schematic of the coupled ocean–atmosphere boundary layer model. Southward wind stress at the ocean–atmosphere interface forces eastward Ekman transport in the atmospheric boundary layer and westward Ekman transport in the oceanic boundary layer. Both boundary layers are assumed to be unstratified with temperature $T^*(x)$ in the ocean and $\Theta^*(x)$ in the atmosphere. The density in the mixed layers connects continuously with stratified interiors through changes in the mixed layer depth. There is a heat flux between the ocean and atmosphere and a specific solar heat flux Q^* into the ocean, and the atmospheric temperature Θ^* is restored back toward a uniform temperature of Θ_r.

here contains elements that are likely to be important in all regions.

2. A simple model for sea surface temperature

We consider a two-dimensional (depth/longitude) eastern boundary region[2] subject to upwelling favorable wind conditions (Fig. 2). The ocean is forced by wind stress and heat flux from the atmosphere. It is assumed that a large-scale pressure field exists in the atmosphere that forces a steady, uniform southward wind. The atmosphere is stably stratified above the boundary layer and unstratified within the boundary layer. Similarly, it is also assumed that there is a well-mixed surface layer in the ocean that overlies a uniformly stratified deep interior. Note that the mixed layer depth is not spatially uniform; it is deeper for colder sea surface temperatures. The southward wind stress will drive an offshore Ekman transport in the ocean, which is compensated by upwelling of cold water in a narrow region near the eastern boundary. This cold water is advected offshore and warmed by heat exchange with the atmosphere. Ekman transport in the atmosphere is onshore, advecting warm air over the cold water.

A steady heat budget integrated over the depth of the ocean mixed layer may be written as a balance between horizontal advection and surface heat flux. Contributions from vertical advection and entrainment have been found to be small in such eastern subtropical gyre regions (Roemmich 1989; Marchesiello et al. 2003; Edwards and Kelly 2007) and will be neglected here. However, some entrainment is implicit in the steady state represented by this model as vertical mixing homogenizes the mixed layer temperature down to its equilibrium depth:

$$U_o T_x^* + V_o T_y^* + F + \frac{\Gamma}{\rho_0 C_p}(T^* - \Theta^*) = \frac{Q^*}{\rho_0 C_p}, \tag{1}$$

where $U_o = uH_o$ and $V_o = vH_o$ are the zonal x and meridional y horizontal transports, T^* is the sea surface temperature, and Θ^* is the temperature in the atmospheric boundary layer. The surface heat flux is composed of a relaxation term proportional to the difference between the ocean and atmospheric temperatures and a specified uniform surface heat flux Q^*. This flux will be referred to as a solar forcing but it is best thought of as a residual between the net surface solar radiation and large-scale meridional heat advection. Also, Γ is a thermal exchange coefficient (in $\mathrm{W\,m^{-2}\,K^{-1}}$), ρ_0 is a

[2] Although the model is configured on an f plane, the orientation will be described here as though it were near an eastern boundary of the ocean.

representative density of seawater, and C_p is the specific heat of seawater. The effects of eddy fluxes are represented by F. Subscripts x and y indicate partial differentiation.

The mixed layer depth $H_o = (\Theta_r - T^*)/T_z^*$ is a function of x. The term Θ_r is the equilibrium temperature for the atmosphere in the absence of the SST influence (discussed more below), and also the background temperature profile at the surface. This mixed layer depth is just the depth at which the SST matches the background temperature profile, consistent with the assumption of an unstratified mixed layer overlying a uniformly stratified interior. Although simple, this mixed layer parameterization is well suited for our problem. The offshore Ekman advection of cool water provides the energy needed for turbulent convection. As the water is warmed by the air–sea heat flux, the mixed layer continuously shallows so that the entrainment fluxes vanish. As will be shown in section 3, this basic structure is also found in more complete numerical models. In the nondimensional framework discussed below, the mixed layer depth is only explicitly represented in the eddy flux term.

The zonal transport is the sum of the Ekman transport and a geostrophic transport. Since the winds are parallel to the boundary the vertically averaged Ekman transport is purely zonal. The geostrophic velocities are composed of the velocity at the base of the mixed layer and the baroclinic shear due to lateral density gradients within the mixed layer. The depth-averaged baroclinic shear within the mixed layer is parallel to the density contours and thus does not advect density, so the influence of the geostrophic velocities is controlled by the velocity at the base of the mixed layer. For simplicity it is assumed that this geostrophic velocity is much less than the Ekman velocity and so it is neglected in the theory. The theory will be compared with a numerical model, which includes these terms, in section 3.

The zonal transport is just the Ekman transport:

$$U_o = \frac{\tau}{\rho_0 f_0}, \tag{2}$$

where τ is the meridional wind stress and f_0 is the constant Coriolis parameter.

Mixed layer instabilities tend to restratify the mixed layer. Although they contribute no net heating when integrated over the mixed layer depth, they do warm the surface and cool the base of the mixed layer. This effect is parameterized following Fox-Kemper et al. (2008):

$$F = \frac{c_e g \alpha_o H_o^2 T_x^{*2}}{\rho_0 f_0}, \tag{3}$$

where c_e is an empirical constant, α_o is the thermal expansion coefficient, and g is the gravitational acceleration.

The surface wind stress is composed of three terms:

$$\tau = \tau_0 \left[1 - \left(\frac{\rho_a C_D}{\tau_0} \right)^{1/2} \frac{\alpha_a g H_a}{f_0} \Theta_x^* \right]^2 + \alpha (T^* - \Theta^*), \tag{4}$$

where τ_0 is the wind stress that would arise if there were no thermal wind shear in the atmospheric boundary layer, ρ_a is a representative density of the atmosphere, C_D is a quadratic drag coefficient, α_a is the thermal expansion coefficient for air, H_a is the boundary layer height, and α is a coefficient that represents the feedback between sea surface temperature and surface wind (Chelton et al. 2004; O'Neill et al. 2005). The surface stress is reduced if the ocean temperature is less than the atmospheric temperature. The second term in brackets is the change in surface wind, and thus the surface stress via the bulk parameterization of Large and Pond (1981), that results through thermal wind if there is a positive horizontal temperature gradient in the atmospheric boundary layer. The actual stress is based on the difference between the atmospheric wind and the ocean current. However, the mean ocean current in these regions is $O(0.1\,\mathrm{m\,s^{-1}})$ while the atmospheric winds are $O(10\,\mathrm{m\,s^{-1}})$ and so the ocean currents are negligible. Although taking eddies into consideration, whose surface velocities are an order of magnitude larger than the mean currents, has been found to significantly reduce the eddy activity in these eastern boundary current regions (Seo et al. 2016; Renault et al. 2016b), such coupling is not included in the model.

This formulation neglects spindown of the Ekman layers in both the atmosphere and ocean. This effect is caused by Ekman pumping into or out of the Ekman layer that modifies the thickness of the boundary layer and thus the horizontal pressure gradients. The net effect is to reduce the wind stress curl compared to what would be found in the absence of this modification. The time over which spindown takes place scales as U_a/L, where U_a is the zonal Ekman velocity in the atmosphere and L is the offshore decay scale of the SST anomaly. If the meridional geostrophic wind is $V_g = O(10\,\mathrm{m\,s^{-1}})$ and the surface stress is $O(0.1\,\mathrm{N\,m^2})$, the Ekman velocity will be $O(1\,\mathrm{m\,s^{-1}})$. This effect is small as long as the meridional length scale of the upwelling favorable winds is less than $V_g L/U_a \approx 10L$. The meridional extent of upwelling favorable winds is generally greater than L but by less than an order of magnitude and so spindown of the Ekman layer will be

neglected. However, this scaling also suggests that this effect may not be entirely negligible.

A heat balance equation can be derived for the atmospheric boundary layer that is similar to that for the ocean but with the solar radiation term replaced by a radiative equilibrium term:

$$U_a\Theta_x^* + \frac{\Gamma}{\rho_a C_{\rm pa}}(\Theta^* - T^*) + \frac{\Gamma_r}{\rho_a C_{\rm pa}}(\Theta^* - \Theta_r) = 0. \quad (5)$$

The first term is the zonal advection of temperature, which is assumed to be due to the Ekman velocity. The second term is the air–sea heat exchange, similar to but of opposite sign to that for the ocean. The final term represents large-scale forcing that maintains the temperature of the atmosphere. It can be interpreted as radiative adjustment (e.g., Barsugli and Battisti 1998) or large-scale advection from upwind. The term Θ_r is the equilibrium temperature for the atmosphere in the absence of the SST influence, and Γ_r is a constant representing the strength of this remote effect (in $\mathrm{W\,m^{-2}\,K^{-1}}$). For upwelling favorable winds, the first term warms the atmosphere and the second and third terms can either cool or warm the atmosphere, depending on the offshore location and the strength of the solar heat flux. The Ekman transport in the atmospheric boundary layer is then

$$U_a = -\frac{\tau}{\rho_a f_0}. \quad (6)$$

The variables in (1) and (5) are nondimensionalized with Θ_r for T^* and Θ^*, and Θ_r/T_z^* for H_o, where T_z^* is the vertical gradient of temperature below the ocean mixed layer. The horizontal length scale used to nondimensionalize x and y is given by

$$L = \frac{\tau_0 C_p}{f_0 \Gamma}. \quad (7)$$

This length scale is simply the distance a parcel would be advected by the Ekman velocity over the time scale at which the ocean SST is restored toward the atmospheric temperature over the mixed layer depth. The resulting equations for the nondimensional T and Θ are

$$(1-\delta\Theta_x)^2 T_x + \epsilon(T-\Theta)T_x + T - \Theta - \mu(1-T)^2 T_x^2 \mathcal{H}(1-T) = Q \quad \text{and} \quad (8a)$$

$$-c(1-\delta\Theta_x)^2\Theta_x + \epsilon c(T-\Theta)\Theta_x + \Theta - T + \gamma(\Theta - 1) = 0. \quad (8b)$$

The nondimensional constants are defined as

$$\epsilon = \frac{\alpha\Theta_r}{\tau_0}\mu = \frac{c_e g \alpha_o \Gamma \Theta_r^3 f_0}{C_p \tau_0^2 T_z^{*2}}\delta = \frac{\alpha_a g H_a}{f_0}\left(\frac{\rho_a C_D}{\tau_0}\right)^{1/2}\Theta_r\left(\frac{\Gamma f_0}{\tau_0 C_p}\right) \quad \text{and} \quad (9a)$$

$$c = C_{\rm pa}/C_p \quad \gamma = \Gamma_r/\Gamma \quad Q = Q^*/\Gamma\Theta_r. \quad (9b)$$

The $(1-T)^2$ term in (8a) is the nondimensional mixed layer depth squared. For $T = 0$ the mixed layer depth, in dimensional units, is $H_o = \Theta_r/T_z^*$ and for $T = 1$ the mixed layer depth is zero. The Heaviside function $\mathcal{H}(1-T)$ sets this term to zero if $T > 1$, which is possible for $Q > 0$. In this case, the mixed layer depth is zero and there is a very thin, warm layer at the surface of the ocean forced by the incoming solar radiation.

Typical values of these nondimensional numbers will be provided below. It is assumed that the coldest water is found at the boundary, $T = 0$ at $x = 0$. This boundary condition is intended to represent the narrow upwelling region whose width is $O(10\,\mathrm{km})$ (e.g., Allen 1980; Samelson and de Szoeke 1988) and much narrower than the offshore decay scale for SST, the focus of this model. Note that Θ_r is the atmospheric temperature relative to sea surface temperature at the boundary; it is not the absolute atmospheric temperature.

These equations represent a nonlinear, coupled system for the interaction between the atmospheric boundary layer and the ocean mixed layer. The model is forced by a radiative heating and large-scale pressure gradient that is in geostrophic balance with an upwelling favorable wind field. The ocean is forced by a surface wind stress, an air–sea heat flux that is proportional to the difference in temperature at the air–sea interface, and a uniform surface heat flux. Nonlinear effects and the nondimensional numbers that characterize their magnitude include feedback between SST and surface wind stress (ϵ), mixed layer instabilities (μ), and thermal wind shear in the atmospheric boundary layer (δ).

Parameter dependencies

1) FIXED ATMOSPHERE, $\gamma = \infty$

Before considering the fully coupled set of equations, solutions are presented for various reduced systems in order to demonstrate the influence of the nonlinear oceanic terms. The ocean effects are most clearly revealed in the limit of infinite heat capacity for the atmosphere ($\gamma = \infty$). This is the limit used by many ocean models in which the ocean SST is restored toward a specified atmospheric temperature that does not change in response to the resulting air–sea heat flux. The atmospheric temperature $\Theta = 1$ in this case.

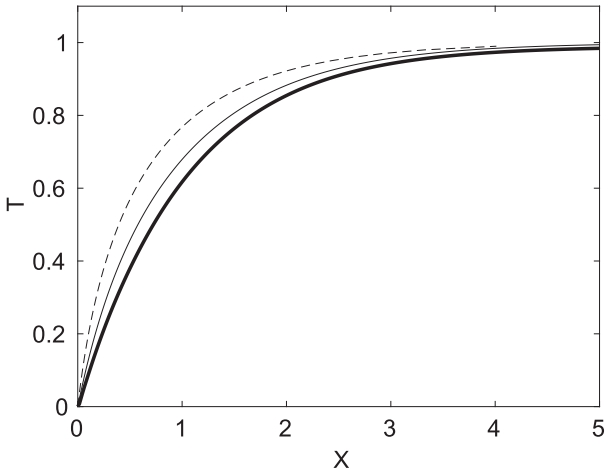

FIG. 3. Nondimensional solutions for SST as a function of offshore distance in the limit of $\gamma = \infty$ and $Q = 0$. The heavy solid line is the linear solution [(10)]; the dashed line is the nonlinear solution including coupling between SST and wind stress [(14)]; the thin black line is the nonlinear solution including a parameterization of baroclinic instability [(17)].

The zeroth-order solution for the ocean, with $\epsilon = \mu = \delta = 0$, is simply

$$T_0 = (1 + Q)(1 - e^{-x}). \tag{10}$$

The ocean temperature approaches its equilibrium temperature of $1 + Q$ exponentially with offshore scale $L = \tau_0 C_p / f_0 \Gamma$ (Fig. 3, bold black line). The length scale is independent of the mixed layer depth because the advective heat flux is inversely proportional to mixed layer depth but the restoring time scale, for fixed restoring strength Γ, is proportional to mixed layer depth. Note that this balance does not require that the Ekman transport be distributed over the mixed layer depth, only that it be entirely within the mixed layer. Because a thin Ekman layer is destabilizing by advecting dense water over light water, the resulting turbulent mixing effectively distributes the lateral advective heat flux over the mixed layer depth even though the velocity may be confined near the surface. The length scale is also independent of the solar heating Q, which is taken to be zero for this figure.

2) SST–WIND STRESS COUPLING, $\epsilon > 0$, $\mu = \delta = 0$, $\gamma = \infty$

Now consider the nonlinear effects of SST on the surface wind. The equation to be solved is

$$T_x + T + \epsilon(T - 1)T_x = 1 + Q. \tag{11}$$

Define $\zeta = T - (1 + Q)$, in which case (11) becomes

$$\zeta_x + \zeta + \epsilon(\zeta + Q)\zeta_x = 0. \tag{12}$$

This can be rearranged as

$$d\zeta[(1 + \epsilon Q)/\zeta + \epsilon] = -dx. \tag{13}$$

Integrating (13), and imposing the boundary condition that $T = 0$, or $\zeta = -(1 + Q)$, at $x = 0$ gives a solution for ζ:

$$\zeta^{(1+\epsilon Q)} e^{\epsilon\zeta} = A e^{-x} \quad A = -(1 + Q)^{(1+\epsilon Q)} e^{-\epsilon(1+Q)}. \tag{14}$$

Although the solution is exact, it is useful to show the basic structure by considering $Q = 0$ and replacing the exponential on the left-hand side with the first two terms in a series expansion in ϵ, appropriate for small ϵ, as

$$e^{\epsilon\zeta} = 1 + \epsilon\zeta + O(\epsilon^2), \tag{15}$$

so that, to $O(\epsilon)$,

$$T = \zeta + 1 \approx 1 + A_1 e^{-x}(1 - \epsilon\zeta) \approx 1 + A_1 e^{-x} - \epsilon A_1^2 e^{-2x}$$
$$A_1 = [1 - (1 + 4\epsilon)^{1/2}]/2\epsilon \tag{16}$$

with the constant A_1 chosen to satisfy the boundary condition $T = 0$ at $x = 0$.

In addition to the original boundary layer, there is a narrower boundary layer of scale $L/2$ that results from the SST–wind feedback. In the absence of solar heating, the amplitude of the primary boundary layer term is decreased ($A_1 \le 1$) compared to the zeroth-order solution, which causes the warm water to shift closer to the eastern boundary. The narrow boundary layer is smaller in amplitude by ϵA_1 and causes a further increased SST gradient near the eastern boundary.

For typical parameters, $\epsilon = \alpha\Theta_r/\tau_0 = 0.5$, with $\alpha = 0.01\,\mathrm{N\,m^{-2}\,K^{-1}}$, $\Theta_r = 5\,\mathrm{K}$, and $\tau_0 = 0.1\,\mathrm{N\,m^{-2}}$. The temperature profile with this nonlinear coupling term and $Q = 0$ is shown in Fig. 3 by the dashed line. The primary influence is to reduce the wind stress, because the upwelled water is cold, which in turn reduces the offshore decay scale of the cold water, because it is proportional to the wind stress. This is consistent with the behavior found in the coupled ocean–atmosphere models of Perlin et al. (2007) and Colas et al. (2013). The influence of the solar forcing will be shown in the following section.

3) MIXED LAYER INSTABILITY, $\mu > 0$, $\epsilon = \delta = 0$, $\gamma = \infty$

The influence of mixed layer instabilities on SST is included through the μ term for $T < 1$. It is assumed that the solution is composed of the zeroth-order term plus a higher-order term proportional to μ. Substituting $T = T_0 + \mu T_1$ into (8a) with $\Theta = 1$ and solving for the $O(\mu)$ terms, the temperature profile is then written as

$$T = A_2(1 - e^{-x}) + \mu[-Q^2A_2^2e^{-2x} + QA_2^3e^{-3x} - 1/3A_2^4e^{-4x} + (1/3A_2^4 - QA_2^3 + Q^2A_2^2)e^{-x}], \quad (17)$$

where $A_2 = 1 + Q$.

For typical parameters, $\mu = c_e g\alpha_o \Gamma \Theta_r^3 f_0 / C_p \tau_0^2 T_z^{*2} = 0.4$, where $\Gamma = 15\,\mathrm{W\,m^{-2}\,K^{-1}}$, $\alpha_o = 0.2\,\mathrm{kg\,m^{-3}\,K^{-1}}$, $\Theta_r = 5\,\mathrm{K}$, $f_0 = 10^{-4}\,\mathrm{s^{-1}}$, $C_p = 4000\,\mathrm{J\,kg^{-1}\,K^{-1}}$, $\tau_0 = 0.1\,\mathrm{N\,m^{-2}}$, $T_z = 0.02\,\mathrm{K\,m^{-1}}$, and $c_e = 0.015$ is an empirical constant.

The influence of mixed layer instability, in the absence of solar heating, is primarily to warm the ocean over a boundary layer of length scale L, with a very narrow boundary layer of width $L/4$ resulting in a larger gradient in SST near the eastern boundary (Fig. 3, thin black line). The eddies make the surface warmer than is found without instabilities. This is consistent with findings from eddy-resolving numerical models (Marchesiello et al. 2003; Capet et al. 2008). Solar radiation results in two additional boundary layers of intermediate width, but they are of smaller magnitude (because $A_2 > Q$).

4) VARIABLE ATMOSPHERE, FINITE γ, $\epsilon = \mu = \delta = 0$

We now allow the heat exchange with the ocean to change the temperature of the atmospheric boundary layer by making γ finite. To obtain analytic solutions the nonlinear terms will not be considered ($\epsilon = \mu = \delta = 0$). The resulting governing Eqs. (8a) and (8b) can be combined into a single equation for T:

$$T_{xx} + (1 - c^{-1} - \gamma/c)T_x - \gamma/cT + \gamma/c(1 + Q) + Q/c = 0, \quad (18)$$

whose solution is

$$T = A_3(1 - e^{-\lambda x})\ A_3 = (1 + \gamma^{-1})Q + 1. \quad (19)$$

There is only one boundary layer that remains bounded for $x = \infty$ given by

$$\lambda = \frac{1}{2}(1 - c^{-1} - \gamma/c) + \frac{1}{2}[(1 - c^{-1} - \gamma/c)^2 + 4\gamma/c]^{1/2}. \quad (20)$$

Note that the solar radiation term does not influence the length scale over which SST varies but it does influence the offshore temperature of both the ocean and the atmospheric boundary layer. The atmospheric temperature is then

$$\Theta = T_x + T - Q = A_3[1 - (1 - \lambda)e^{-\lambda x}] - Q. \quad (21)$$

The parameter c is the ratio of the specific heat of air to that of seawater, which is approximately 0.25. The only remaining parameter is $\gamma = \Gamma_r/\Gamma$, the ratio of the restoring strength for the atmosphere toward Θ_r to the restoring strength of the SST to the atmospheric temperature.

Barsugli and Battisti (1998) estimate the value of Γ_r by linearizing a one-dimensional radiative damping term as

$$\Gamma_r = 4\epsilon_a\sigma_B(2\Theta^3 - T^3) \approx 4\epsilon_a\sigma_B\Theta^3, \quad (22)$$

where $\epsilon_a = 0.76$ is the atmospheric longwave emissivity and $\sigma_B = 5.67e^{-8}\,\mathrm{W\,m^{-2}\,K^{-4}}$ is the Stefan–Boltzmann constant. For an ocean temperature that is within a few degrees of the atmospheric temperature, the approximation on the right-hand side provides a useful order of magnitude estimate for the restoring strength. For $\Theta = 289°\,\mathrm{K}$ (where now Θ is absolute temperature), the damping term $\Gamma_r = O(4\,\mathrm{W\,m^{-2}\,K^{-1}})$. This is larger than found for the full depth atmosphere, which is typically $O(2\,\mathrm{W\,m^{-2}\,K^{-1}})$ (e.g., Stephens et al. 1981) because the effective atmospheric temperature over the full depth of the atmosphere is much cooler than the atmospheric temperature near the ocean surface. The coupling strength between the ocean and atmosphere $\Gamma = O(10\,\mathrm{W\,m^{-2}\,K^{-1}})$ (Seager et al. 1995; Frankignoul et al. 1998). It is noted, however, that there is much uncertainty in both these numbers and they depend on the spatial scale of the anomalies (Marotzke and Pierce 1997) so we consider γ as an only weakly constrained parameter and seek to understand how its value influences the solution.

The solutions for a range of γ (with $Q = 0$) are shown in Fig. 4. For $\gamma = 5$, strong atmospheric restoring, the decay scale is only slightly larger than that for $\gamma = \infty$ (cf. solid and dotted lines in Fig. 4a). The atmosphere is cooled near the boundary but remains as warm as $0.8\Theta^*$ at the boundary. For $\gamma = 1$, the offshore decay scale increases and the temperature of the atmosphere decreases. For $\gamma = 0.1$ the cold water extends very far offshore compared to the $\gamma = \infty$ case and the atmospheric temperature is nearly the same as the ocean temperature. In this limit it takes a great distance offshore in order to provide enough heat flux from the atmosphere (and ultimately from the radiative heating of the atmosphere) in order to warm the cold upwelled water in the ocean. This is only partially due to the difference in heat capacity of the ocean compared to the atmosphere. The primary contributing factor is that, for small γ, the atmospheric boundary layer temperature gets cold and so the heat flux from the atmosphere to the ocean decreases, prolonging the distance a parcel would need to be advected in order to reach its equilibrium temperature.

There are several useful limits that can be inferred from these solutions. In all cases, the offshore

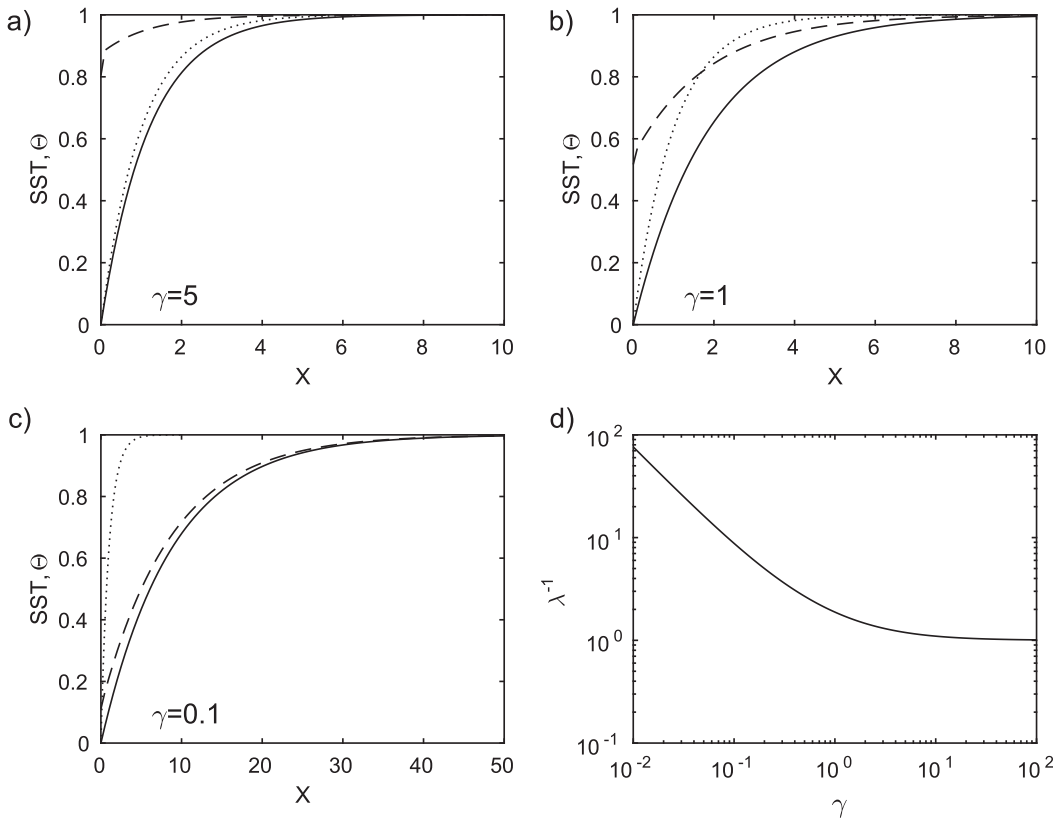

FIG. 4. Solutions for the coupled set of Eqs. (19) and (21) for (a) $\gamma = 5$, (b) $\gamma = 1$, and (c) $\gamma = 0.1$. The solid line is the SST, the dashed line is the atmospheric boundary layer temperature, and the dotted line is the linear solution for $\gamma = \infty$. (d) The nondimensional length scale of the boundary layer as a function of γ. The length scale becomes very long for $\gamma \ll 1$ (weak atmospheric restoring).

equilibrium state is such that $T - \Theta = Q$. In the absence of solar radiation, the ocean surface temperature asymptotes to the atmospheric temperature Θ_r. For $Q \gg 1$ and $\gamma \gg 1$ (strong heating and strong SST restoring) $A_3 = Q$ and far offshore $T^* = Q^*/\Gamma$ and $\Theta^* = 0$ (in dimensional units). For strong heating and weak restoring, $A_3 = Q/\gamma$, $T^* = \Theta_r + Q^*/\Gamma_r$ and $\Theta^* = Q^*/\Gamma_r$ (in dimensional units). With solar radiation the ocean far offshore becomes warmer than the atmosphere and the net solar heat flux is balanced by a sensible heat flux back into the atmospheric boundary layer. As the air–sea coupling gets weak ($\gamma \ll 1$), the ocean must get very warm in order to provide enough outgoing heat flux to balance the incoming solar radiation.

The boundary layer decay scale λ^{-1} is shown in Fig. 4d. Asymptotic solutions for (20) show that for $\gamma \gg 1$, the decay scale approaches 1. This is the same limit previously discussed for $\gamma = \infty$ where the offshore decay scale is $L = \tau_0 C_p/\Gamma f_0$. For weak restoring in the atmosphere, $\gamma \ll 1$, the decay scale approaches γ^{-1}. In dimensional units, this is $\tau_0 C_p/\Gamma_r f_0$, which becomes very large as the atmospheric restoring strength Γ_r gets weak. So for strong air–sea coupling the decay scale is set by the ocean, for weak coupling the decay scale is set by the atmosphere, and for realistic coupling [$\gamma = O(1)$] both the ocean and atmosphere determine the decay scale.

5) NONLINEAR COUPLED SYSTEM: FINITE $\gamma, \delta, \epsilon = \mu = 0$

The imprint of cold SST on the temperature of the atmospheric boundary layer introduces a nonlinear effect because the thermal wind associated with the lateral gradient of Θ will reduce the southward flow from the top of the boundary layer to the surface. This will in turn reduce the surface stress and the Ekman transport in both fluids, and thus affect the equilibrium heat balance. For a typical marine boundary layer, $\rho_a = 1.3\,\mathrm{Kg\,m^{-3}}$, $C_D = 0.001$, $\tau_0 = 0.1\,\mathrm{N\,m^{-2}}$, $C_p = 4000\,\mathrm{J\,Kg^{-1}\,K^{-1}}$, $\Gamma = 10\,\mathrm{W\,m^{-2}\,K^{-1}}$, $\alpha_a = 0.003\,\mathrm{Kg\,m^{-3-1}}$, $H_a = 10^3\,\mathrm{m}$, and $\Theta^* = 6°\mathrm{C}$, which gives $\delta = 0.75$. The coupled Eqs. (8a) and (8b) with $\epsilon = \mu = Q = 0$ and $\delta = 0.75$ are integrated numerically. The SST and atmospheric temperature are compared to the case with $\delta = 0$ (no thermal wind in the atmospheric boundary layer) in

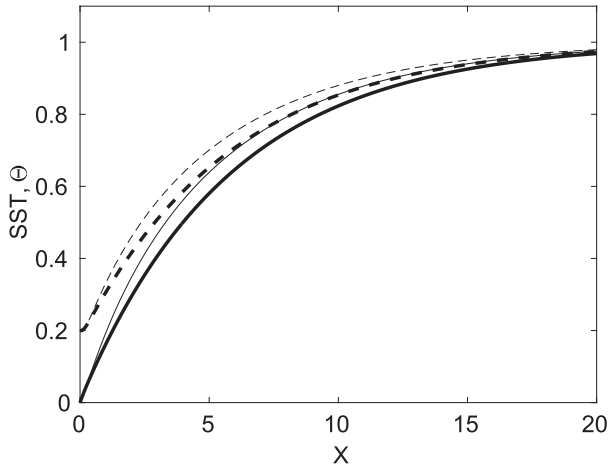

FIG. 5. The nonlinear influence of thermal wind in the atmosphere with $\gamma = 0.25$. Bold lines are for $\delta = 0$ and thin lines for $\delta = 0.75$. Solid lines are ocean SST; dashed lines are atmospheric boundary layer temperature Θ.

Fig. 5. Thermal wind makes both the ocean and the atmosphere slightly warmer in the interior and increases the horizontal gradients near the boundary.

3. Comparisons with a numerical model

The analytic model in the previous section has the advantage of providing simple, closed-form solutions with a clear representation of the physical processes that control SST. However, the model requires numerous assumptions and simplifications and it remains to be seen whether or not the dominant length scale predicted by the theory is found in more complete systems. A primitive equation numerical ocean model is now used to test the theory in applications ranging from two-dimensional linear configurations to three-dimensional ones with baroclinic instability and a basin-scale wind-driven gyre.

The model is the Massachusetts Institute of Technology general circulation model (MITgcm), which solves the primitive equations on a Cartesian grid in the horizontal and on depth coordinates in the vertical (Marshall et al. 1997). The model is run in both two-dimensional (longitude and depth) and three-dimensional domains. The atmospheric temperature is specified, so these calculations are equivalent to the $\gamma = \infty$ limit. For the two-dimensional calculations, the model is forced by applying a uniform southward wind stress of magnitude τ_0 and by restoring the uppermost model temperature toward a spatially uniform atmospheric temperature Θ^* with a time scale $\rho_0 C_p h_1/\Gamma = 30$ days, which is equivalent to a restoring strength of $\Gamma = 15.8\,\mathrm{W\,m^{-2}\,K^{-1}}$. In several cases a uniform surface heat flux is also imposed. The horizontal resolution is 4 km and the vertical resolution is 10 m. The zonal extent of the basin is 1536 km and there is a flat bottom at 300-m depth. Calculations with a topographic slope near the boundary are essentially the same as those reported here (not shown). The Coriolis parameter is nominally $10^{-4}\,\mathrm{s^{-1}}$ and constant (although its value will be varied). Within 100 km of the offshore boundary the temperature is restored with a time scale of 30 days toward its initial profile of uniform stratification ($N^2 = 4 \times 10^{-5}\,\mathrm{s^{-2}}$; surface temperature of $\Theta^* = 16.2$°C).

This provides a source of deep cold water to balance the heating at the surface and allows for equilibrium solutions to be obtained. Subgrid-scale mixing of momentum is parameterized with a vertical viscosity of $10^{-4}\,\mathrm{m^2\,s^{-1}}$, Smagorinsky Laplacian horizontal viscosity with nondimensional coefficient 2.5, and a quadratic bottom drag with coefficient 0.003. The vertical diffusion coefficient for temperature is $10^{-5}\,\mathrm{m^2\,s^{-1}}$ under stable density profiles but is increased to $10^{3}\,\mathrm{m^2\,s^{-1}}$ under unstable density profiles, effectively mixing density to be uniform in the vertical.

To test the influence of a horizontal gyre circulation and Rossby waves, the model is also configured in a 4000 km × 4000 km square basin with a Coriolis parameter that varies from $0.6 \times 10^{-4}\,\mathrm{s^{-1}}$ at the southern boundary to $1.4 \times 10^{-4}\,\mathrm{s^{-1}}$ at the northern boundary ($\beta = 2 \times 10^{-11}\,\mathrm{m^{-1}\,s^{-1}}$). For these basin-scale calculations the atmospheric temperature varies linearly with latitude as $\Theta^* = \Theta_0^* + \Theta_y^* y$, with $\Theta_0^* = 20.4$°C and $\Theta_y = -1.25 \times 10^{-6}\,\mathrm{°C\,m^{-1}}$, giving a north–south change in temperature of 5°C. A wind-driven subtropical gyre is also added through the curl of the zonal wind stress as $\tau = \tau_0 \cos(\pi y/L_y)\mathbf{i} + \tau_0 \mathbf{j}$, where L_y is the meridional extent of the basin, $\tau_0 = -0.1\,\mathrm{N\,m^{-2}}$, and $\mathbf{i}$ and $\mathbf{j}$ indicate the zonal and meridional unit vectors. This gives an Ekman pumping rate in the center of the gyre of $25\,\mathrm{m\,yr^{-1}}$, which is consistent with the annual mean Ekman pumping rate in the subtropical eastern Pacific (Huang and Qiu 1994). The horizontal resolution is 10 km and the basin depth is increased to 1000 m with the vertical grid spacing increasing from 10 m in the upper 150 m to 100 m near the bottom. The initial stratification was decreased to $N^2 = 2 \times 10^{-5}\,\mathrm{s^{-2}}$. There is no full depth restoring of the stratification; the only buoyancy forcing is the restoring of the uppermost model temperature to Θ^* with a time scale of 30 days.

a. *Two-dimensional solutions*

The two-dimensional model was run with $\tau_0 = -0.1\,\mathrm{N\,m^{-2}}$ and $Q = 0$ for a period of 1000 days to ensure that the fields are at steady state. A vertical

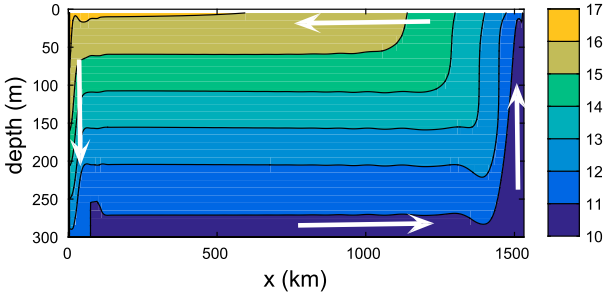

FIG. 6. Zonal section of temperature (°C) from the two-dimensional numerical model calculation with $Q^* = 0$. The circulation is indicated schematically by the white arrows.

section of temperature is shown in Fig. 6. Cold water is upwelled along the eastern boundary, where the mixed layer extends to the bottom. The surface water warms offshore and the mixed layer shallows, approximately to the depth of each isotherm in the interior stratification. The region near the western boundary is warmed due to the downwelling driven by the Ekman transport at the surface but is transformed into the specified interior stratification by the full depth restoring term near the boundary. This pattern is generally consistent with the schematic upon which the analytic model was constructed (Fig. 2). Also note that the Ekman transport is confined to a much shallower depth than the mixed layer but that the lateral heat transport is distributed over the full mixed layer depth due to vertical mixing.

The SST as a function of offshore distance is shown in Fig. 7a by the blue line. It increases from approximately 11°C at the eastern boundary to 16.2°C over a horizontal length scale of $O(500)$ km. A series of other model calculations was carried out in which the parameters were varied as follows: $\tau = -0.075\,\mathrm{N\,m^{-2}}$, $-0.125\,\mathrm{N\,m^{-2}}$; $f_0 = 0.5 \times 10^{-4}\,\mathrm{s^{-1}}$, $2 \times 10^{-4}\,\mathrm{s^{-1}}$; $\Gamma = 8\,\mathrm{W\,m^{-2}\,K^{-1}}$, $47\,\mathrm{W\,m^{-2}\,K^{-1}}$, $N^2 = 1.75 \times 10^{-5}\,\mathrm{s^{-2}}$, $1 \times 10^{-5}\,\mathrm{s^{-2}}$, and $Q = 50, 75$, and $100\,\mathrm{W\,m^{-2}}$. In each of these cases the other parameters were the same as in the original calculation (so that only one variable was changed at a time), the resulting SST is shown in Fig. 7a by the thin black lines. The horizontal decay scale, temperature of the upwelled water, and temperature in the interior vary between each of these calculations. Those cases with solar radiation equilibrate at temperatures warmer than Θ_r.

These model SST distributions were nondimensionalized as $T = (T - T_{\min})/[(1 + Q)(\Theta^* - T_{\min})]$, where $T_{\min}$ was diagnosed from the model calculation as the SST at the eastern boundary (which was always close to the coldest water in the interior). The solar radiation has been included in this scaling so that the offshore decay scale, the main quantity of interest here, is more clearly evident for those cases with solar radiation. The offshore distance was scaled by $L = \tau_0 C_p/\Gamma f_0$, as in the analytic theory. The resulting SST profiles in Fig. 7b all collapse onto a single curve (solid lines) consistent with the theory (dashed line). The dot-dashed line is a calculation using the KPP vertical mixing parameterization (Large et al. 1994) but is otherwise the same as the blue line in Fig. 7a. The SST is nearly identical to the theory and the cases with simple vertical convection parameterization.

The feedback of SST on surface wind stress can also be represented in the numerical model. The wind stress was modified as $\tau = \tau_0[1 + \alpha(T - \Theta^*)]$, where T is the model SST and $\alpha = 0.01\,\mathrm{N\,m^{-2}\,K^{-1}}$ represents the strength of the feedback. The SST values in these cases are shown in Fig. 7c by the thin solid lines. The SSTs in the standard cases with no feedback are given by the thick solid lines. The SSTs predicted by the theory (14) are given by the dashed lines. The agreement between the model and theory is good, and confirms that the essential response of the upper ocean to such air–sea coupling is a warming of the upper ocean and a narrowing of the region of SST gradient. The approximate solution with $Q = 0$, (16), is indicated by the black dash-dotted line, which is in close agreement with the theory and exact solution, confirming the double boundary layer structure of the coupled solution.

The influence of baroclinic instability is now considered using a three-dimensional configuration of the numerical model. The meridional extent of the domain is extended to 400 km with periodic boundary conditions in the meridional direction. The initial conditions and forcing are the same as for the standard case, although the model grid spacing has been reduced to 2 km in order to better resolve the instabilities. The nondimensional SST is compared to the two-dimensional case in Fig. 7d. The main effect of the baroclinic instability is to slightly warm SST in the region of steep SST gradient just offshore of the eastern boundary. Baroclinic instability may be more important in the real ocean because there is significant baroclinic shear at depths below the mixed layer, forced by processes that are not in the present theory. Baroclinic shear is produced in the theory solely by lateral gradients in SST and mixed layer depth.

b. *Subtropical gyre*

The theory neglects contributions to the upper ocean heat budget that arise due to advection by the wind-driven gyre, meridional gradients in SST, and baroclinic Rossby waves. While it is difficult to include these in any general way in the theory, the numerical model can be configured to include each of these effects. The model domain was extended to 4000 km in both the zonal and meridional directions and the anticyclonic wind stress

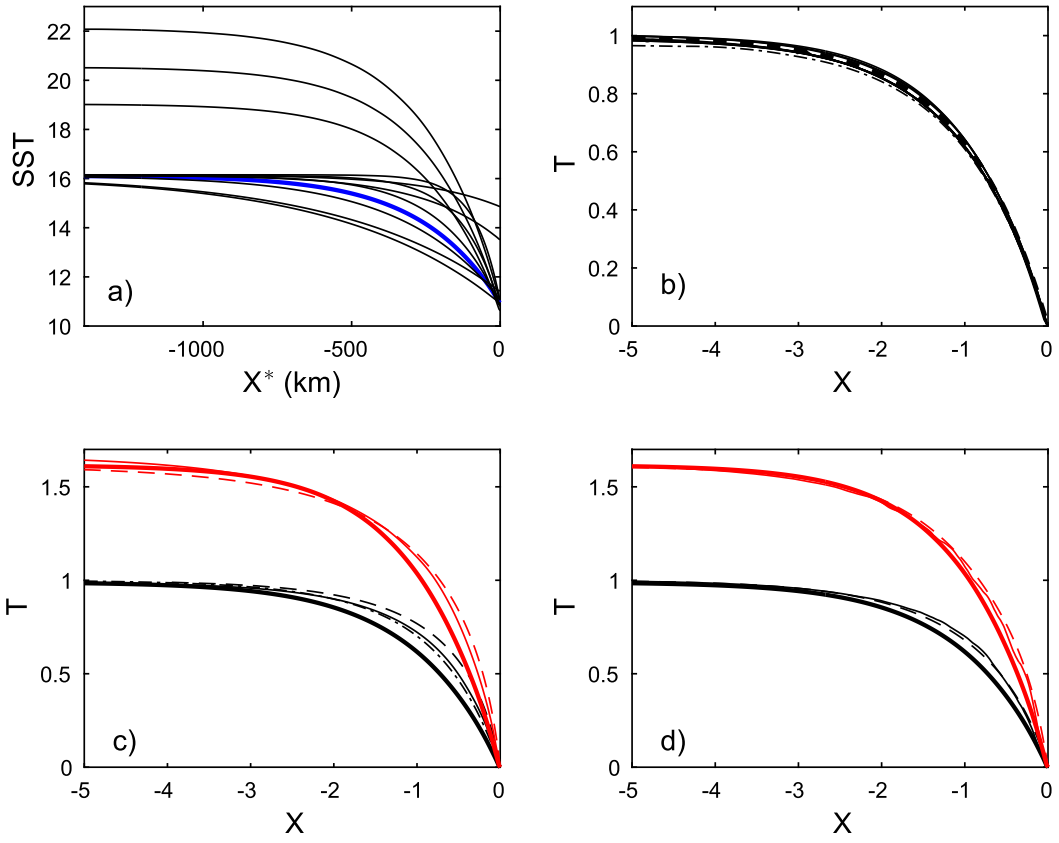

FIG. 7. Comparison between the theory and the two-dimensional ocean model. (a) Dimensional SST (°C) for a series of model runs in which τ_o, Γ, f_0, Q, and N^2 were varied. The blue line is the calculation in Fig. 6. (b) Nondimensional SST from the model (solid lines) and the theory [(10)] (dashed line). The dot-dashed line is the same calculation as in Fig. 6 except with KPP mixing parameterization in the vertical. (c) Influence of coupling between SST and surface wind stress. The thick solid lines are no coupling, thin solid lines are the model with coupling, dashed lines are the theory with coupling [(14)], and the dash-dotted line is the approximate solution [(16)]. Black lines are for $Q = 0$ and red lines are for $Q = 0.6$. (d) Influence of baroclinic instability. The thick solid lines are the two-dimensional SST from the model, thin solid lines are the meridional average from three-dimensional calculations that includes baroclinic instability, the dashed lines are the theory [(17)], black lines are for $Q = 0$, and red lines are for $Q = 0.6$.

curl defined above was added to the uniform meridional wind stress. There are several additional processes now included that are not considered in the theory. There is meridional advection of SST by the wind-driven gyre due to both the meridional dependence of the offshore decay scale and the meridional gradient in Θ^*. There are also Doppler shifts due to the zonal component of the wind-driven gyre and the zonal geostrophic flow associated with the meridional gradient in SST. Finally, this calculation also includes the influences of the westward propagation of thermal anomalies on a β plane, which, in the longwave limit, will propagate at βL_d^2, where L_d is the baroclinic deformation radius based on the mixed layer depth. The model was run for a period of 55 years, with the mean quantities diagnosed over the final 5 years of simulation. This configuration was run with both $Q^* = 0$ and $Q^* = 75\,\mathrm{W\,m^{-2}}$. The mean SST for the case with $Q^* = 0$ is shown in Fig. 8a. There is a meridional gradient in SST over most of the middle of the domain forced by $\Theta^*(y)$. Upwelling boundary layers on the northern and southern boundaries are also evident, as is the northward advection of warm water in the western boundary current. Near the eastern boundary the isotherms turn toward the south, giving rise to a region of cold water extending several hundred kilometers offshore.

This cold region near the eastern boundary is driven by the southward meridional wind stress. It is not a natural consequence of the anticyclonic wind stress curl that drives the subtropical gyre, nor is it due to the meridional gradient in Θ^*. This is demonstrated by the mean SST for a calculation that is otherwise identical but with no meridional wind stress (Fig. 8b). The interior and western boundary regions are similar to the case with the meridional winds but there is no cold region near the eastern

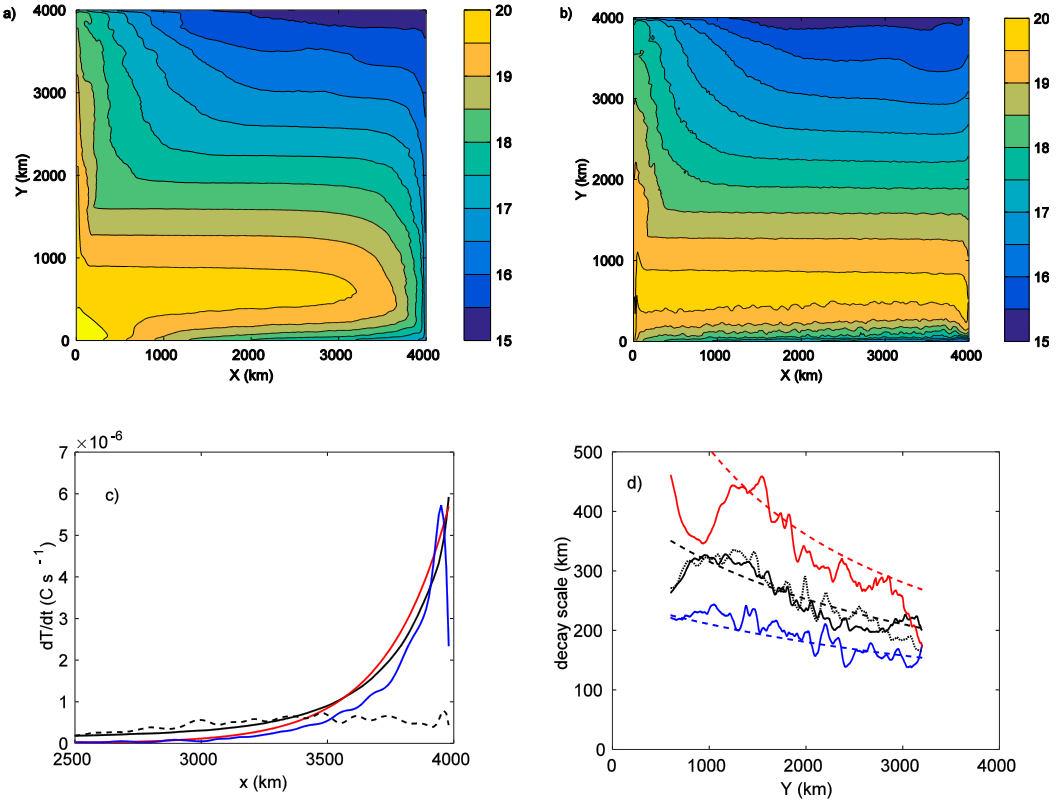

FIG. 8. (a) Mean SST (°C) from a numerical model calculation with uniform meridional winds, a subtropical gyre driven by the meridional gradient of zonal winds, and a meridional gradient in atmospheric temperature. (b) As in (a), for a case with no meridional winds. (c) Terms in the temperature budget integrated over the mixed layer depth and averaged between $y = 1500$ km and $y = 2500$ km: surface heat flux (black), zonal advection (blue), meridional advection (dashed), and surface heat flux from the theory (red). (d) Decay scale diagnosed by an exponential fit to the mean model SST at each latitude with $Q^* = 0$ (solid lines) and that predicted by the theory (dashed lines). The black dotted line is with $Q^* = 75\,\mathrm{W\,m^{-2}}$. The Coriolis parameter at the midlatitude of the basin is $1.0 \times 10^{-4}\,\mathrm{s^{-1}}$ [black, as shown in (a) and (c)], $0.7 \times 10^{-4}\,\mathrm{s^{-1}}$ (red), and $1.4 \times 10^{-4}\,\mathrm{s^{-1}}$ (blue).

boundary. The weak, very narrow boundary layer evident (cold in the south, warm in the north) is due to the no-normal-flow condition on the eastern boundary and thermal damping of the westward propagating Rossby wave (Davey 1983; Spall 2003). This boundary layer scales as $\beta L_d^2 H_o \rho_0 C_p / \Gamma^2$, where L_d is the baroclinic deformation radius. If we take $L_d = 10$ km for the mixed layer depth anomalies, this gives a boundary layer width of $O(50\,\mathrm{km})$, which is consistent with that found in Fig. 8b and much less than that found in Fig. 8a. This is how Rossby waves influence the offshore extent of density anomalies from the eastern boundary and the relatively narrow boundary layer width justifies its neglect in the theory.

The surface heat loss in the model, averaged between $y = 1500$ km and $y = 2500$ km, is shown in Fig. 8c. This compares well with the theory (red line) taken at the midlatitude of the basin. The primary assumption of the theory, that the surface heat loss is balanced by the zonal advection of temperature, is also supported by this calculation. The zonal advection term greatly exceeds the meridional advection term in the eastern boundary region where the SST gradient is the largest. The offshore decay scale diagnosed from the model, which is $O(200 - 300\,\mathrm{km})$, agrees reasonably well with that predicted by the theory, at least away from the northern and southern boundaries of the domain (Fig. 8d). The decay scale diagnosed from the case with $Q^* = 75\,\mathrm{W\,m^{-2}}$ is given by the black dotted line. It is very similar to that found for $Q^* = 0$ and supports the theoretical prediction that the decay scale is independent of the solar heat flux. The latitudinal dependence of the offshore decay scale is clear, but this is due to the decrease in Ekman velocity at higher latitudes, not because Rossby waves are slower at higher latitudes. This conclusion is supported by additional calculations in which the Coriolis parameter was increased and decreased compared to the central case (colored lines in Fig. 8d). If the offshore decay scale were controlled by Rossby wave propagation it would scale as f^{-2} instead of f^{-1} as found here.

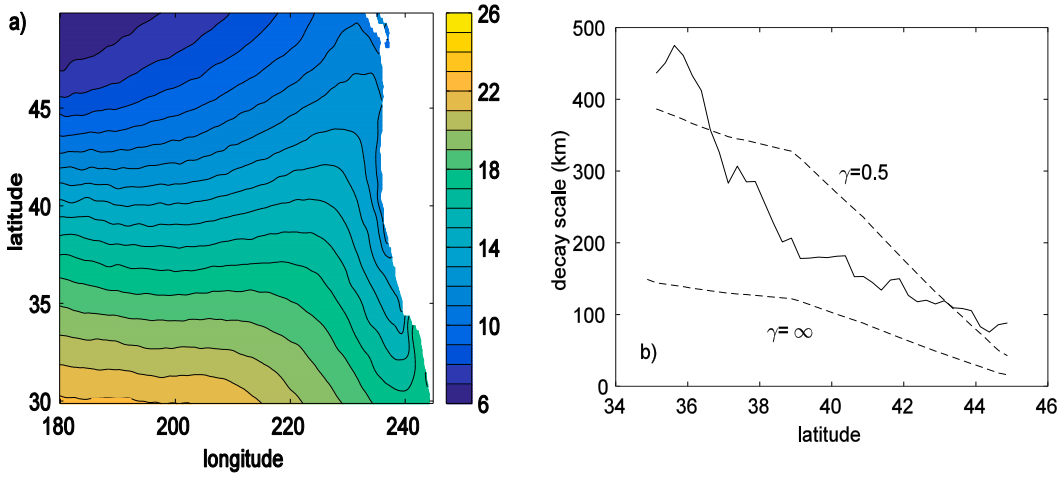

FIG. 9. (a) Sea surface temperature (°C) from the annual mean NOAA SST in the eastern North Pacific. (b) The offshore decay scale diagnosed from (a) (solid line) and the decay scale predicted by the linear, coupled theory [(19)] with $\gamma = 0.5$ (upper dashed line) and $\gamma = \infty$ (lower dashed line).

4. Comparison to climatological SST

The annual mean NOAA SST in the eastern North Pacific Ocean is shown in Fig. 9a.[3] The cold water along the eastern boundary and its decay offshore are evident. To compare with the theory, a nondimensional temperature anomaly, relative to the minimum found near the eastern boundary, was calculated as a function of latitude between 35° and 45°N. The temperature is scaled by the difference between the coldest water on the boundary and the warmest water offshore, and so varies between 0 at the coast and 1 in the interior. An exponential profile was fit to each of these curves (Fig. 9b). The average of R^2 calculated at each latitude was 0.82, so the exponential decay provides a reasonably good fit to the climatological SST. The offshore decay scale ranges between 100 km and 400 km and decreases with increasing latitude.

The offshore decay scale predicted by the linear, coupled system (19) is now compared to that in the NOAA SST data. The wind stress is calculated from the NCEP 10-m wind monthly climatology between 1981 and 2010[4] using the Large and Pond (1981) algorithm. The maximum southward wind stress along the eastern boundary is calculated each month and then averaged in time. The resulting mean southward wind stress along the eastern boundary varies almost linearly between about 0.03 N m^{-2} at 35°N and 0.004 N m^{-2} at 45°N. The neglect of seasonal and spatial variations in wind stress and SST is a strong assumption since the advective time scale for the Ekman transport is of the same order of magnitude as the seasonal time scale. However, the goal here is only to provide a check to see that the offshore decay is roughly exponential and that the magnitude and spatial dependence are consistent with that predicted by the theory.

The decay scale is shown in Fig. 9b for two choices of γ. The upper dashed line is for $\gamma = 0.5$, which is similar to the estimate based on the linearized radiation balance of Barsugli and Battisti (1998). The lower dashed line is for $\gamma = \infty$, equivalent to a fixed atmospheric temperature. The length scale predicted by the theory decreases with increasing latitude, generally consistent with that diagnosed from the NOAA SST climatology. The weak increase at low latitudes in the theory is a result of the mean NCEP wind stress becoming nearly constant at these same latitudes. Although these length scale estimates for both the theory and the climatology are somewhat sensitive to various choices, such as averaging period, wind stress, and value of γ, this result supports the general prediction of the theory, namely that the observed SST anomaly decays roughly exponentially offshore, that the decay scale decreases with increasing latitude, and that it is of the same order of magnitude as that predicted by the linear, coupled theory.

5. Summary

There is strong coupling between the ocean and atmosphere in eastern ocean basins at subtropical latitudes. High pressure over the cool open ocean and low pressure over the warm continent result in upwelling favorable (equatorward) winds. This drives offshore Ekman transport, which in turn upwells cold waters

[3] Data and processing details are available online at http://www.esrl.noaa.gov/psd/data/gridded/data.noaa.oisst.v2.highres.html.

[4] Available online at http://www.esrl.noaa.gov/psd/data/gridded/data.ncep.reanalysis.html.

from below and gives rise to cold sea surface temperatures, high nutrients, and productive ecosystems. These cold temperatures moderate away from the boundary but their influence can be seen extending hundreds of kilometers offshore. The atmosphere responds to this cold surface water by developing low-level stratocumulus clouds, which partially reflect the incoming solar radiation. Even with this cloud cover, however, these regions represent a significant heat sink for the atmosphere. Global climate models have a difficult time accurately representing this coupled system with large warm biases in SST, insufficient cloud cover, and incorrect heat exchange and precipitation (Richter 2015; Large and Danabasoglu 2006).

The primary goal of this study is the development of a basic theory for the coupled ocean–atmosphere system under such upwelling conditions. The model couples an upper ocean mixed layer with an atmospheric boundary layer subject to momentum and heat exchange at the air–sea interface. The system is forced by an imposed, large-scale southward wind, a restoring of the atmospheric temperature toward a warm background state, solar radiation into the ocean, and a restoring of the ocean temperature toward a stratified interior far offshore. The fundamental length scale over which the cold SST signal penetrates into the interior is revealed by a simple linear model for the ocean with a fixed atmospheric temperature. This length scale $L = \tau_0 C_p/\Gamma f_0$ is the distance a parcel would be advected by the ocean Ekman velocity over a thermal damping time scale. The theory was extended to consider the weakly nonlinear influences of SST on surface wind, baroclinic instability in the ocean, and thermal wind in the atmospheric boundary layer. A linear theory for the coupled system shows that the cold anomalies will extend farther offshore than for a fixed atmospheric temperature because the cooling of the atmospheric boundary layer reduces the air–sea heat flux. For typical parameters, this length scale is several hundred kilometers.

The theory was compared to a series of numerical model calculations ranging from two-dimensional and steady to three-dimensional, time dependent, and eddy-resolving. Processes included in the model but neglected by the theory include explicit vertical stratification, baroclinic instability, a subtropical gyre circulation, meridional gradient in the planetary vorticity, and meridional gradient in the atmospheric temperature. Despite these additional physical processes, the eastern boundary region of the model develops an exponential decay of cold SST that is roughly in agreement with that predicted by the theory. Climatological SST anomalies along the west coast of the United States also show a roughly exponential decay offshore with a length scale that agrees reasonably well with the theory.

The results of this study support that the cold SST found in eastern ocean subtropical gyres is a result of the coupled ocean–atmosphere system. The basic offshore decay scale is inherent to the ocean but it is significantly modified by processes in the atmosphere. Specifically, the radiant heat balance in the atmosphere strongly modulates the offshore extent of the cold water. As the radiant heating to balance the ocean cooling weakens the offshore extent of the cold water greatly increases. This is because, as the ocean is more able to cool the atmospheric boundary layer, the air–sea heat exchange, which is proportional to the temperature difference at the air–sea interface, decreases. This reduced heat flux allows the cold water to be advected farther offshore by the Ekman transport.

The theory developed here is very idealized and neglects several processes that are likely to be important in at least some regions of the world's oceans. Baroclinic instability arising from gradients in mixed layer density was found to warm the surface near the boundary but was relatively unimportant farther offshore. In reality there are additional baroclinic currents in eastern boundary regions that are not considered here and are likely to increase the importance of eddy fluxes to the overall heat budget, as are found in realistic high resolution models (e.g., Colas et al. 2012). Geostrophic advection has also been neglected but for sufficiently strong gyre circulations or meridional gradients in SST this term may also become important. Rossby wave effects were also found to be small but will rapidly increase in importance at lower latitudes. The theory presented here is best viewed as an objective starting point, complimentary to other more complex models and data analysis, from which to understand the dynamics of the coupled ocean–atmosphere system eastern basins.

Acknowledgments. MAS was supported by the Andrew W. Mellon Foundation Endowed Fund for Innovative Research and the National Science Foundation under Grant OCE-1433170 and PLR-1415489. NS was supported by the National Aeronautics and Space Administration under Grant NNX14AL83G, the Department of Energy, Office of Science Grant DE-SC0006766, and the Japan Agency for Marine-Earth Science and Technology as part of the JAMSTEC-IPRC Joint Investigations. Joseph Pedlosky is thanked for helping with the nonlinear solutions for SST–wind stress coupling. Comments and suggestions from anonymous reviewers helped improve the presentation.

The University of Hawaii is thanked for logistical and travel support for MAS to visit the university, during which time most of this work was done.

REFERENCES

Allen, J. S., 1980: Models of wind-driven currents on the continental shelf. *Annu. Rev. Fluid Mech.*, **12**, 389–433, doi:10.1146/annurev.fl.12.010180.002133.

Barsugli, J. J., and D. S. Battisti, 1998: The basic effects of atmosphere–ocean thermal coupling on midlatitude variability. *J. Atmos. Sci.*, **55**, 477–493, doi:10.1175/1520-0469(1998)055<0477:TBEOAO>2.0.CO;2.

Capet, X., P. Marchesiello, and J. McWilliams, 2004: Upwelling response to coastal wind profiles. *Geophys. Res. Lett.*, **31**, L13311, doi:10.1029/2004GL020123.

——, F. Colas, J. McWilliams, P. Penven, and P. Marchesiello, 2008: Eddies in eastern-boundary subtropical upwelling systems. *Ocean Modeling in an Eddying Regime*, *Meteor. Monogr.*, Vol. 177, Amer. Geophys. Union, 131–147, doi:10.1029/177GM10.

Chelton, D. B., M. G. Schlax, M. H. Freilich, and R. F. Milliff, 2004: Satellite measurements reveal persistent small-scale features in ocean winds. *Science*, **303**, 978–983, doi:10.1126/science.1091901.

——, ——, and R. M. Samelson, 2007: Summertime coupling between sea surface temperature and wind stress in the California Current System. *J. Phys. Oceanogr.*, **37**, 495–517, doi:10.1175/JPO3025.1.

Colas, F., J. C. McWilliams, X. Capet, and J. Kurian, 2012: Heat balance and eddies in the Peru–Chile Current system. *Climate Dyn.*, **39**, 509–529, doi:10.1007/s00382-011-1170-6.

——, X. Capet, J. C. McWilliams, and Z. Li, 2013: Mesoscale eddy buoyancy flux and eddy-induced circulation in eastern boundary currents. *J. Phys. Oceanogr.*, **43**, 1073–1095, doi:10.1175/JPO-D-11-0241.1.

Davey, M. K., 1983: A two-level model of a thermally forced ocean basin. *J. Phys. Oceanogr.*, **13**, 169–190, doi:10.1175/1520-0485(1983)013<0169:ATLMOA>2.0.CO;2.

Dorman, C. E., E. P. Dever, J. Largier, and D. Koračin, 2006: Buoy measured wind, wind stress and wind stress curl over the shelf off Bodega Bay, California. *Deep-Sea Res. II*, **53**, 2850–2864, doi:10.1016/j.dsr2.2006.07.006.

Edwards, K. A., and K. A. Kelly, 2007: Seasonal heat budget across the extent of the California Current. *J. Phys. Oceanogr.*, **37**, 518–530, doi:10.1175/JPO2990.1.

Fox-Kemper, B., R. Ferrari, and R. Hallberg, 2008: Parameterization of mixed layer eddies. Part I: Theory and diagnosis. *J. Phys. Oceanogr.*, **38**, 1145–1165, doi:10.1175/2007JPO3792.1.

Frankignoul, C., A. Czaja, and B. L'Heveder, 1998: Air–sea feedback in the North Atlantic and surface boundary conditions for ocean models. *J. Climate*, **11**, 2310–2324, doi:10.1175/1520-0442(1998)011<2310:ASFITN>2.0.CO;2.

Holte, J., F. Straneo, J. T. Farrar, and R. A. Weller, 2014: Heat and salinity budgets at the stratus mooring in the southeast Pacific. *J. Geophys. Res. Oceans*, **119**, 8162–8176, doi:10.1002/2014JC010256.

Huang, R. X., and B. Qiu, 1994: Three-dimensional structure of the wind-driven circulation in the subtropical North Pacific. *J. Phys. Oceanogr.*, **24**, 1608–1622, doi:10.1175/1520-0485(1994)024<1608:TDSOTW>2.0.CO;2.

Large, W. G., and S. Pond, 1981: Open ocean momentum flux measurements in moderate to strong winds. *J. Phys. Oceanogr.*, **11**, 324–336, doi:10.1175/1520-0485(1981)011<0324:OOMFMI>2.0.CO;2.

——, and G. Danabasoglu, 2006: Attribution and impacts of upper-ocean biases in CCSM3. *J. Climate*, **19**, 2325–2346, doi:10.1175/JCLI3740.1.

——, J. C. McWilliams, and S. C. Doney, 1994: Oceanic vertical mixing: A review and a model with a nonlocal boundary layer parameterization. *Rev. Geophys.*, **32**, 363–403, doi:10.1029/94RG01872.

Marchesiello, P., J. C. McWilliams, and A. Shchepetkin, 2003: Equilibrium structure and dynamics of the California Current system. *J. Phys. Oceanogr.*, **33**, 753–783, doi:10.1175/1520-0485(2003)33<753:ESADOT>2.0.CO;2.

Marotzke, J., and D. W. Pierce, 1997: On spatial scales and lifetimes of SST anomalies beneath a diffusive atmosphere. *J. Phys. Oceanogr.*, **27**, 133–139, doi:10.1175/1520-0485(1997)027<0133:OSSALO>2.0.CO;2.

Marshall, J., C. Hill, L. Perelman, and A. Adcroft, 1997: Hydrostatic, quasi-hydrostatic, and non-hydrostatic ocean modeling. *J. Geophys. Res.*, **102**, 5733–5752, doi:10.1029/96JC02776.

McCreary, J. P., Y. Fukamachi, and P. K. Kundu, 1991: A numerical investigation of jets and eddies near an eastern ocean boundary. *J. Geophys. Res.*, **96**, 2515–2533, doi:10.1029/90JC02195.

O'Neill, L. W., D. B. Chelton, S. K. Esbensen, and F. Wentz, 2005: High-resolution satellite measurements of the atmospheric boundary layer response to SST variations along the Agulhas return current. *J. Climate*, **18**, 2706–2723, doi:10.1175/JCLI3415.1.

Pedlosky, J., 1978: An inertial model of steady coastal upwelling. *J. Phys. Oceanogr.*, **8**, 171–177, doi:10.1175/1520-0485(1978)008<0171:AIMOSC>2.0.CO;2.

Perlin, N., E. D. Skyllingstad, R. M. Samelson, and P. L. Barbour, 2007: Numerical simulation of air–sea coupling during coastal upwelling. *J. Phys. Oceanogr.*, **37**, 2081–2093, doi:10.1175/JPO3104.1.

Renault, L., A. Hall, and J. C. McWilliams, 2016a: Orographic shaping of US West Coast wind profiles during the upwelling season. *Climate Dyn.*, **46**, 273–289, doi:10.1007/s00382-015-2583-4.

——, M. J. Molemaker, J. C. McWilliams, A. F. Shchepetkin, F. Lemarie, D. Chelton, S. Illig, and A. Hall, 2016b: Modulation of wind work by oceanic current interaction with the atmosphere. *J. Phys. Oceanogr.*, **46**, 1685–1704, doi:10.1175/JPO-D-15-0232.1.

Richter, I., 2015: Climate model biases in the eastern tropical oceans: Causes, impacts and ways forward. *Wiley Interdiscip. Res.: Climatic Change*, **6**, 345–358, doi:10.1002/wcc.338.

Roemmich, D., 1989: Mean transport of mass, heat, salt and nutrients in the southern California coastal waters: Implications for primary production and nutrient cycling. *Deep-Sea Res.*, **36**, 1359–1378, doi:10.1016/0198-0149(89)90088-5.

Samelson, R. M., and R. A. de Szoeke, 1988: Semigeostrophic wind-driven thermocline upwelling at a coastal boundary. *J. Phys. Oceanogr.*, **18**, 1372–1383, doi:10.1175/1520-0485(1988)018<1372:SWDTUA>2.0.CO;2.

Seager, R., Y. Kushnir, and M. A. Cane, 1995: On heat flux boundary conditions for ocean models. *J. Phys. Oceanogr.*, **25**, 3219–3230, doi:10.1175/1520-0485(1995)025<3219:OHFBCF>2.0.CO;2.

Seo, H., A. J. Miller, and J. R. Norris, 2016: Eddy–wind interaction in the California Current System: Dynamics and impacts. *J. Phys. Oceanogr.*, **46**, 439–459, doi:10.1175/JPO-D-15-0086.1.

Spall, M. A., 2003: Islands in zonal flow. *J. Phys. Oceanogr.*, **33**, 2689–2701, doi:10.1175/1520-0485(2003)033<2689:IIZF>2.0.CO;2.

Stephens, G. L., G. G. Campbell, and T. H. Vonder Haar, 1981: Earth radiation budgets. *J. Geophys. Res.*, **86**, 9739–9760, doi:10.1029/JC086iC10p09739.